

THE INITIAL STATE OF HEAVY ION COLLISIONS

Javier L. Albacete

*CAFPE and Departamento de Física Teórica y del Cosmos
Universidad de Granada, E-18071, Granada, Spain
albacete@ugr.es*

Adrian Dumitru

*RIKEN BNL Research Center, Brookhaven National Laboratory, Upton, NY 11973, USA
Department of Natural Sciences, Baruch College, CUNY,
17 Lexington Avenue, New York, NY 10010, USA
The Graduate School and University Center, The City University of New York,
365 Fifth Avenue, New York, NY 10016, USA
adrian.dumitru@baruch.cuny.edu*

Cyrille Marquet

*Centre de Physique Théorique, École Polytechnique, CNRS, 91128 Palaiseau, France
cyrille.marquet@cern.ch*

We present a brief review of recent theoretical developments and related phenomenological approaches for understanding the initial state of heavy ion collisions, with emphasis on the Color Glass Condensate formalism.

Keywords: Heavy Ion Collisions; Color Glass Condensate; High energy QCD.

PACS numbers:

1. Introduction

One of the major challenges since the discovery of QCD has been to understand hadronic Fock-space wave functions in the high-energy limit. It was realized long ago that due to the soft singularity of the splitting function of non-Abelian gauge bosons, hadronic wave functions would contain a large number of gluons with a small (light-cone) momentum fraction x .¹ This expectation was confirmed by $e + p$ deep-inelastic scattering experiments at HERA (see below) and led to the replacement of early gluon distributions with little “small- x glue”, such as the Duke-Owens distribution with $xg(x) \approx \text{const}$ at $Q^2 = 4 \text{ GeV}^2$, by modern PDFs like CTEQ with a high density of gluons at low x .

The growth of the gluon density with decreasing x (or increasing rapidity) implies that at sufficiently high energy non-linear dynamics of the soft color fields would emerge. That is, the increase of the gluon density within a rapidity step from

2 Authors' Names

Y to $Y + \Delta Y$ is no longer simply proportional to the number of gluons that were already present at Y ,^{1,2} or else unitarity is violated eventually. Instead, the scattering amplitude is thought to *saturate* at some *dynamically generated* virtuality scale $Q_s(Y)$ which increases with rapidity. This new phenomenon is commonly referred to as *saturation* of gluon distributions at low x and manifests in non-linear, density dependent terms in the QCD evolution equations. Furthermore, high gluon densities enhance the role of multiparton interactions during the collision process, known as *higher twists* in the context of collinear factorization. At moderate transverse momentum multiple scatterings may become a leading effect and should be resummed to all orders, which implies a rearrangement of the perturbative series.

The saturation momentum Q_s is boosted further in heavy nuclei due to the fact that the density of large- x “valence” charges per unit transverse area increases in proportion to the thickness $\sim A^{1/3}$ of a nucleus.³⁻⁵ These represent the sources for the small- x soft gluon fields. Thus, non-linear color field dynamics should be operative at higher transverse momentum scales than for nucleons. Investigating the gluon structure of a hadron or nucleus at low x is of fundamental interest, and this can be well done using e+p, e+A and p+A collisions. Understanding the dynamics of small- x gluons in nuclei is also a crucial factor in determining the initial state of a heavy ion (A+A) collision right after impact. This is the aspect which we emphasize in this review, with a perspective on the latest results from the LHC heavy-ion program.

Different approaches have been developed to study initial state effects, we shall focus on the Color Glass Condensate (CGC) formalism while briefly discussing alternatives in parallel. Knowing the density and distribution of gluons that have been released is necessary for a complete dynamical description of the collision before the eventual thermalization of the system and the formation of a Quark Gluon Plasma (QGP). The practical implications are many. In the soft sector, say particles with small transverse momentum $p_t \lesssim 1$ GeV, the initial conditions determine the bulk features of multiparticle production in heavy ion collisions such as dN/dy or dE_T/dy as a function of collision energy, the collision geometry (distribution of produced gluons in the transverse plane) and so on. A very important application of the CGC formalism is to provide such initial conditions for the subsequent evolution. This input affects significantly the transport coefficients such as shear viscosity extracted from hydrodynamic analysis of heavy-ion collisions. Also, it gives rise to non-trivial long-range correlations in rapidity and to density “hot spots” which are visible in final-state azimuthal correlations.

In the “hard probes” sector, i.e. for particles with a –perturbatively– large transverse momentum that do not thermalize but are used as tomographic probes, a proper distinction of initial state effects from those due to the QGP (“final state effects”) is vital for a quantitative characterization of the matter produced in heavy ion collisions as they may sometimes lead to qualitatively similar phenomena in observables of interest.

Last but not least, another primary goal of studies of the initial state is to

provide proof that (local) thermalization of the system actually happens over the time scales estimated from hydrodynamical simulations, $\tau_{therm} \sim 0.5 \div 1 \text{ fm}/c$. How such ultra-fast isotropization of the system happens is, arguably, one of the most fundamental open problems in the field of heavy ions.

One important lesson learned from experimental data collected in Au+Au and Pb+Pb collisions at RHIC and the LHC, respectively, is that bulk particle production in ion-ion collisions is very different from a simple superposition of nucleon-nucleon collisions. This is evident, for instance, from the measured charged particle multiplicities which exhibit a strong deviation from scaling with the number of independent nucleon-nucleon collisions: $\frac{dN^{AA}}{d\eta}(\eta = 0) \ll N_{coll} \frac{dN^{NN}}{d\eta}(\eta = 0)$. One is led to the conclusion that strong coherence effects among the constituent nucleons, or the relevant degrees of freedom at the sub-nucleon level, must be present during the collision process. The fact that coherence effects are essential for the description of data is confirmed by the fact that most –if not all– successful phenomenological approaches include them in one form or another. In a QCD description, coherence effects can be related to the presence of large gluon densities both prior to the collision and during the collision process itself^a.

2. Color Glass Condensate

2.1. A Brief review

The CGC is formulated as an effective theory for the small- x degrees of freedom in high-energy QCD scattering. It relies on a separation of degrees of freedom into soft, small- x gluons –treated as dynamical gauge fields– and high- x , static valence degrees of freedom (in terms of light-cone time). The latter act as random sources for the small- x gluons. Any physical observable is averaged over all the possible configurations of the sources according to a probability distribution $W[\rho]_Y$. The fact that the averaging is performed at the level of the observable reflects the fact that at very high energy the hadron is probed in a *frozen* configuration and, hence, interferences between different field configurations are neglected. This is thus an essentially classical picture.

The CGC is endowed with a set of non-linear renormalization group equations –the B-JIMWLK equations^{6–11}– for the probability distribution of the valence sources. This ensures that observables do not depend on the particular momentum scale at which the separation between soft (dynamical) and valence (static) degrees of freedom is performed. The B-JIMWLK equations account for quantum corrections and, at leading logarithmic accuracy, they resum terms $\sim \alpha_s \ln(1/x)$ to all orders. They also include non-linear terms that, in the proper gauge, can be interpreted as due to gluon-gluon recombination processes. The mere presence of non-linear terms immediately implies that a dynamical transverse momentum scale emerges, the saturation scale Q_s , such that gluon modes with transverse momentum

^aWe note that distinguishing before or after the collision is a gauge dependent statement.

4 Authors' Names

$k_t \lesssim Q_s(x)$ are in the saturation regime.

Saturation of gluon densities is equivalent to the presence of strong color fields, parametrically of the order of the inverse of the coupling, $\mathcal{A}(x) \sim 1/g$. Thus, although the insertion of new sources in diagrams for particle production appears to be suppressed by powers of the coupling constant, this is compensated by the strength of the color fields, i.e. terms of the order $g\mathcal{A}(x) \sim \mathcal{O}(1)$ must be resummed to all orders. This implies a rearrangement of the perturbative series in the high-density regime or equivalently, to an all-order resummation of multiple scatterings. The propagation of an energetic projectile, e.g. a quark, moving along the z^- (light-cone) direction, at some transverse position z_\perp in the background of the strong field of a nucleus, denoted A , is conveniently described in terms of Wilson lines by (we are using the $A^- = 0$ gauge):

$$U(z_\perp) = \mathcal{P} \exp \left[ig \int dz^- A^+(z^-, z_\perp) \right]. \quad (1)$$

Wilson lines resum multiple scatterings in the eikonal approximation (neglecting the recoil of the projectile) and they are the relevant degrees of freedom in the high energy regime, rather than *free* quarks or gluons. Actually, the B-JIMWLK equations can be recast as an infinite hierarchy of coupled, non-linear differential equations for the rapidity ($Y \equiv \ln(1/x)$) evolution of n-point correlators of Wilson lines, i.e. for correlators of the type $\langle U(x_{\perp 1}) \dots U(x_{\perp n}) \rangle_Y$. The B-JIMWLK equations are difficult to solve numerically and to implement in phenomenological applications. In turn, the BK equation,^{12,13} which corresponds to the large- N_c limit of the full B-JIMWLK hierarchy and provides a single, closed evolution equation for the 2-point function, $\langle U(x_{\perp 1}) U^\dagger(x_{\perp 2}) \rangle_Y$, is much easier to solve in practice and is widely used in phenomenological applications. As we shall discuss in detail below, the precise prescription for the resummation of multiple interactions varies depending on the observable of interest or the colliding system, and does not always result in easy-to-use factorizable expressions.

A different approach to particle production at high transverse momentum assumes collinear factorization of heavy ion collisions as a working hypothesis. In this framework all nuclear effects –and in particular nuclear shadowing at small- x – are absorbed into modified nuclear parton distribution functions (nPDF's) fitted to experimental data; the scale dependence is described by DGLAP evolution. A variety of intermediate approaches can be found in the literature that start from the collinear factorization ansatz and further extend it to account for multiple scatterings through the calculation of higher twists, in the coherent case, or through an all order resummation of incoherent, Glauber like scatterings. The result of these calculations is sometimes recast in the form of modified nPDF's which include an energy-dependent intrinsic transverse momentum and momentum broadening. Further, cold nuclear matter energy loss is sometimes included in these formalisms. These essentially perturbative tools are complemented with non-perturbative models for soft particle production in Monte Carlo event generators such as HIJING¹⁴ or

HYDJET.¹⁵ There, phase-space arguments motivate the implementation of energy-dependent transverse momentum cut-offs (analogous, in essence, to the CGC saturation scale) in order to regulate independent particle production from different sources in the hard sector. A detailed compilation of such different approaches can be found in.¹⁶

2.2. Theory Status

Despite the intrinsic difficulty of performing perturbative calculations in the background of a strong color field, steady progress in the degree of accuracy of the CGC formalism has been achieved over the last years. Briefly, it can be said that the CGC is now entering the next-to-leading (NLO) order era.

Thus, the kernel of the BK equation is now known to NLO accuracy in the resummation parameter,¹⁷ $\alpha_s \ln(1/x)$ or, through an all-orders resummation of a partial subset of NLO corrections, to running coupling accuracy.^{18–20} The BK equation including running coupling corrections (henceforth referred to as rcBK equation) reads

$$\frac{\partial \mathcal{N}_F(r, x)}{\partial \ln(x_0/x)} = \int d^2 \underline{r}_1 K^{run}(\underline{r}, \underline{r}_1, \underline{r}_2) [\mathcal{N}_F(r_1, x) + \mathcal{N}_F(r_2, x) - \mathcal{N}_F(r, x) - \mathcal{N}_F(r_1, x) \mathcal{N}_F(r_2, x)] , \quad (2)$$

where $\mathcal{N}_F(r = |\underline{z}_1 - \underline{z}_2|, x) = 1 - \frac{1}{N_c} \langle tr [U(\underline{z}_1) U^\dagger(\underline{z}_2)] \rangle_{Y=\ln 1/x}$ is the (imaginary part of) dipole scattering amplitude in the fundamental representation, and $\underline{r}_2 = \underline{r} - \underline{r}_1$. x_0 is some initial scale and K^{run} is the evolution kernel including running coupling corrections. Different prescriptions have been proposed in the literature for K^{run} . As shown in ref.²⁰ Balitsky's prescription minimizes the role of higher *conformal* corrections:

$$K^{run}(\mathbf{r}, \mathbf{r}_1, \mathbf{r}_2) = \frac{N_c \alpha_s(r^2)}{2\pi^2} \left[\frac{1}{r_1^2} \left(\frac{\alpha_s(r_1^2)}{\alpha_s(r_2^2)} - 1 \right) + \frac{r^2}{r_1^2 r_2^2} + \frac{1}{r_2^2} \left(\frac{\alpha_s(r_2^2)}{\alpha_s(r_1^2)} - 1 \right) \right] . \quad (3)$$

Analogous effort has been dedicated to improve the degree of accuracy of the expressions for particle production processes. Thus, a full NLO generalization of the dipole factorization formula for the calculation of structure functions in deep inelastic scattering (DIS) at small- x is now available.^{21, 22} It should be noted, though, that the AAMQS fits reported below were performed using the LO dipole formalism. Also, corrections (sub-leading in density) to the McLerran-Venugopalan action that provide a theoretical justification for the AAMQS parametrization of the initial conditions of the evolution (see below) have been recently calculated.²³

In the case of proton-nucleus collisions there are two distinct but related approaches to single hadron production in the CGC framework: k_t -factorization and the *hybrid* formalism. Their applicability depends on the kinematic region in which the projectile proton is probed: small- x or high- x respectively. In both cases explicitly factorized expressions in terms of *only* the 2-point function or, equivalently, the

unintegrated gluon distribution, are well established. Actually, running coupling, and full NLO corrections to the k_t -factorization and hybrid formalisms have been calculated in²⁴ and²⁵ respectively. However only the *inelastic* corrections –a subset of the full NLO corrections– to the hybrid formalism calculated in²⁶ have been implemented in phenomenological works.^{27,28} These first studies on the impact of the *inelastic* correction indicate that they are sizable²⁸ and, in some cases, they overwhelm the LO contribution in certain kinematic regions (high p_t), which calls for a phenomenological study of the full NLO corrections.

The knowledge of the 2-point function provided by the BK equation does not suffice to describe more exclusive observables. Rather, knowledge of higher point functions, and hence of solutions of the B-JIMWLK equations are needed. An extensive study of the different correlators involved in the calculation of two-particle production processes (di-jet or photon-jet) in p+A collisions and DIS was presented in.²⁹ While the techniques for solving the B-JIMWLK equations numerically have been known for some time, their application remains somewhat difficult. Significant progress has been made recently in devising approximate analytical solutions for arbitrary n -point functions based on the Gaussian truncation of the B-JIMWLK hierarchy,^{30–33} thus extending the semi-classical MV model for the initial condition to evolved systems. This new technique allows to express arbitrary n -point functions in term of the BK-evolved 2-point function thus opening new avenues for a systematic phenomenological exploration of multigluon correlations in available data. A first application of the Gaussian approximation to the study of di-hadron correlations at RHIC can be found in³⁴ where the role of double parton interactions –important for the analysis of di-hadron correlations data–in the CGC has also been investigated.

In the more intricate case of nucleus-nucleus collisions all leading terms in the calculation of inclusive particle production can be resummed by solving the classical Yang-Mills equations of motion (CYM), with the valence degrees of freedom of the two colliding nuclei acting as external non-dynamical sources. However, supplementing the classical methods with information on the quantum evolution of the wave function of the colliding nuclei, necessary to extrapolate from RHIC to LHC energies, is presently a difficult task since, again, it requires the numerical resolution of the full B-JIMWLK equations. This difficulty is bypassed in the IP-Glasma model,³⁵ where B-JIMWLK evolution is replaced by the empiric parametrization of the saturation scale obtained through the IP-Sat model fit to HERA data. Nevertheless, a proof of factorization of inclusive gluon production and multigluon correlators including quantum corrections has been provided in.^{36,37} Those results provide a dynamical framework for the Glasma flux tube picture and provide a rigorous theoretical basis for the study of long range in rapidity correlations in the CGC framework, as we discuss below.

Finally, intense effort has been devoted to the problem of thermalization in heavy ion collisions in the recent years. It has been recently demonstrated in ref.³⁸ that the resummation of the leading secular terms in the evolution of a scalar ϕ^4 theory

coupled to a strong external source makes the pressure tensor of the system relax to its equilibrium value, a prerequisite for the onset of hydrodynamical flow. An equivalent result for QCD would provide a proof of thermalization of the system and may allow to determine the equilibration time as a function of the natural scales of the problem (collision energy, energy density etc). For a recent review on this topic see, e.g.³⁹

Finally, it is worth remarking that the substantial theoretical progress reported above has not been yet fully exploited in phenomenological applications, which leaves a large margin for improvement in the analysis of the upcoming LHC data.

3. e+p to e+A collisions

Despite the fact that CGC effects are expected to be enhanced in nuclei versus protons, which is due to the larger valence charge densities per unit transverse area in nuclei, so far the most exhaustive searches for the gluon saturation phenomenon have been performed using data on proton reactions. This is mainly due to the large body of high quality DIS data on protons at small- x . Moreover, most –if not all– phenomenological approaches for heavy ion collisions borrow empiric information from the analysis of e+p data, either to parametrize the Bjorken- x or energy dependence of the saturation scale or to also constrain more exclusive features of the unintegrated gluon distribution of the proton.

A first analysis of DIS data in terms of saturation physics was provided by the GBW model.⁴⁰ There, a good description of data was obtained with a saturation scale $Q_{s,N}^2(x) = \left(\frac{x_0}{x}\right)^{0.288} \text{ GeV}^2$ with $x_0 = 3 \cdot 10^{-4}$. Such empiric parametrization found a theoretical justification in the analysis of the collinearly improved Leading and Next to Leading BFKL evolution in the presence of saturation boundaries performed in.⁴¹ Other analytic models that explicitly include saturation or unitarity constraints and which also incorporate features of BFKL dynamics, like the IIM model,⁴² or are based on eikonalization of leading twist scattering in the collinear factorization formalism like the IP-Sat model,⁴³ also provided a good description of the data^b and are frequently used for phenomenology.

An important step forward towards a theory driven analysis of the data was brought about by the AAMQS global fits^{45,46} to inclusive structure functions measured in e+p. The AAMQS approach relies on the LO dipole model plus the rcBK evolution equation to describe the small- x dependence of the dipole scattering amplitude, $\mathcal{N}(r, x)$. The free parameters in the AAMQS fits, aside from a global normalization constant and an infrared parameter related to the argument of the running coupling (see⁴⁶ for full details), correspond to the free parameters in the initial

^bFor a recent fit of the IP-sat model to the final data from HERA, including some processes which probe the impact parameter dependence of the dipole scattering amplitude, we refer to ref.⁴⁴ Such modern models do a good job of describing the growth of the gluon density towards low x mentioned already in the introduction.

conditions for the evolution, as follows:

$$\mathcal{N}(r, x = x_0 = 0.01) = 1 - \exp \left[-\frac{(r^2 Q_{s0, \text{proton}}^2)^\gamma}{4} \ln \left(\frac{1}{\Lambda r} + e \right) \right]. \quad (4)$$

Here, $\Lambda = 0.241$ GeV, $Q_{s0, \text{proton}}$ is the saturation scale at the initial x_0 and γ is a dimensionless parameter that controls the steepness of the unintegrated gluon distribution for momenta above the initial saturation scale $k_t > Q_{s0}$. With this set up, the AAMQS fits provide a remarkably good description of data, see Fig. (1) right. Although the AAMQS fits clearly favor values $\gamma > 1$, they do not uniquely determine its optimal value (and neither does the analysis of forward RHIC data performed in ref.⁴⁷). Rather, different pairs of $(Q_{s0, \text{proton}}^2, \gamma)$ -values provide comparably good values of $\chi^2/d.o.f \sim 1$, see Table 1. The “degeneracy” is due to correlations among parameters and also because HERA data is too inclusive to constrain exclusive features of the proton UGD. A recent comparative study of the stability of standard DGLAP and rcBK fits to small- x HERA data under changing boundary conditions performed by systematically excluding subsets of data from the fits showed that rcBK fits do provide more robust fits to data.²⁸ This is an additional indication for the relevance of non-linear small- x dynamics in the analysis of HERA data.

Set	$Q_{s0, \text{proton}}^2$ (GeV ²)	γ
MV	0.2	1
h	0.168	1.119
h'	0.157	1.101

The main obstacle to extending the above studies to the case of nuclear DIS is the paucity of experimental data at small- x . This lack of empiric information to constrain the non-perturbative parameters in either the collinear factorization or CGC formalisms (mostly related to the initial conditions for the evolution) is one of the main sources of uncertainty in nPDF parametrizations (see Fig. 1 right) and in CGC predictions for the LHC. It should be noted that for nuclear targets one additional variable is needed to properly characterize the wave function: the impact parameter dependence. This difficulty is bypassed in standard nPDF minimum bias fits. A first b -dependent nPDF set has been proposed recently in.⁴⁸ In CGC approaches one normally relates the b -dependence of the nuclear saturation scale to the proton saturation scale and the local nuclear density: $Q_{sA}^2(b) = T_A(b) Q_{s, \text{proton}}^2$. This can be done at different levels of refinement: assuming a homogeneous nucleus, a nucleus with a Woods-Saxon density distribution without fluctuations, or, finally, also accounting for geometry fluctuations as in the KLN-MC^{49, 50} and rcBK-MC^{28, 51} Monte Carlo's. Such ansatz, when combined with the AAMQS parameters $\gamma > 1$ (see Table 1) may pose problems as it violates the additivity of nuclear dipole amplitudes on the number of nucleons at small dipole sizes. In order to fix this problem, alternative dependencies of $Q_{sA}^2(b)$ on $T_A(b)$ were explored in ref.²⁸ Data

from the p -Pb run at the LHC will provide important input for sorting out such uncertainties and to get a better determination of nuclear wave functions.

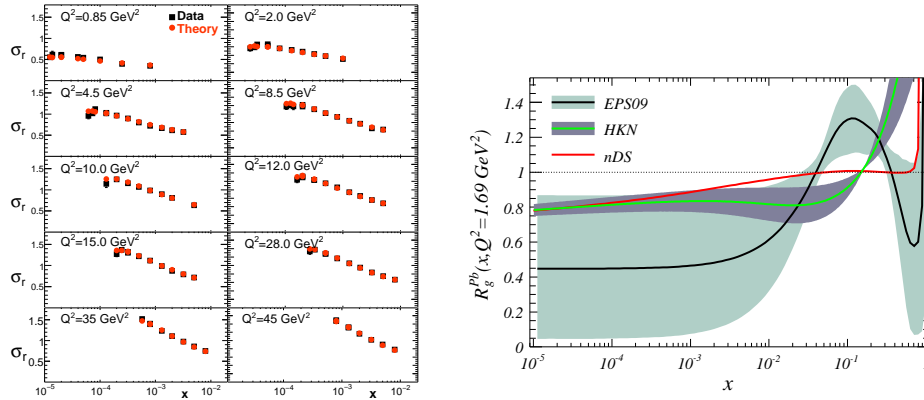


Fig. 1. Left: rcBK fits to HERA data on the reduced cross section in e+p scattering at small- x from.⁴⁶ Right: Different nPDF parametrizations for the nuclear gluon distribution⁵² at $Q^2 = 1.69$ GeV².

4. p+A collisions

Proton nucleus collisions provide a better handle on initial state and gluon saturation effects than those of heavy ions. This is mainly due to the absence of final state effects induced by the presence of a QGP. There are two distinct but related approaches to hadron production in high energy asymmetric (such as proton-nucleus or very forward proton-proton and nucleus-nucleus) collisions. In such collisions, particle production processes in the central rapidity region probe the wave function of both projectile and target at small values of x and can be described in terms of the k_t -factorization formalism where the differential cross-section for inclusive gluon production in A+B collisions is given by⁵³

$$\frac{d\sigma^{A+B \rightarrow g}}{dy d^2p_t d^2R} = K^k \frac{2}{C_F} \frac{1}{p_t^2} \int^{p_t} \frac{d^2k_t}{4} \alpha_s(Q) \int d^2b \varphi\left(\frac{|p_t + k_t|}{2}, x_1; b\right) \varphi\left(\frac{|p_t - k_t|}{2}, x_2; R - b\right), \quad (5)$$

where y , p_t and R are the rapidity, transverse momentum and transverse position of the produced gluon, $x_{1(2)} = (p_t/\sqrt{s_{NN}}) \exp(\pm y)$ and $C_F = (N_c^2 - 1)/2N_c$. The relevant UGD's for the k_t -factorization formula above are given by

$$\varphi(k, x, \mathbf{R}) = \frac{C_F}{\alpha_s(k) (2\pi)^3} \int d^2\mathbf{r} e^{-i\mathbf{k}\cdot\mathbf{r}} \nabla_{\mathbf{r}}^2 \mathcal{N}_A(r, x, \mathbf{R}) \quad (6)$$

where \mathcal{N}_A is the dipole amplitude in the adjoint representation which, in the large- N_c -limit, is related to the dipole amplitude in the fundamental representation by $\mathcal{N}_A(r, x, \mathbf{R}) = 2\mathcal{N}_F(r, x, \mathbf{R}) - \mathcal{N}_F^2(r, x, \mathbf{R})$

However, at more forward rapidities the proton is probed at larger values of x while the target nucleus is deeper in the small- x regime. In that context k_t -factorization fails to grasp the dominant contribution to the scattering process. Rather, the *hybrid* formalism proposed in⁵⁴ is more appropriate. In the hybrid formalism the large- x degrees of freedom of the proton are described in terms of usual parton distribution functions (pdf's) of collinear factorization with a scale dependence given by DGLAP evolution equations, while the small- x glue of the nucleus is still described in terms of its UGD. At leading order, inclusive particle production is given by:

$$\frac{dN^{pA \rightarrow hX}}{d\eta d^2k} = \frac{1}{(2\pi)^2} \int_{x_F}^1 \frac{dz}{z^2} \left[\sum_q x_1 f_{q/p}(x_1, Q^2) \tilde{N}_F \left(x_2, \frac{p_t}{z} \right) D_{h/q}(z, Q^2) + x_1 f_{g/p}(x_1, Q^2) \tilde{N}_A \left(x_2, \frac{p_t}{z} \right) D_{h/g}(z, Q^2) \right], \quad (7)$$

where

$$\tilde{N}_{F(A)}(k, x, \mathbf{R}) = \int d^2\mathbf{r} e^{-i\mathbf{k}\cdot\mathbf{r}} [1 - \mathcal{N}_{F(A)}(r, x, \mathbf{R})]. \quad (8)$$

Next-to-leading corrections to Eq. (7) have been calculated in.^{25,26} Clearly, the *hybrid* formalism is restricted to production of particles with high enough transverse momentum, as implied by its use of collinear factorized pdf's and fragmentation functions. Unfortunately, no smooth matching between the k_t -factorization and *hybrid* formalisms is known to date. Also, their corresponding limits of applicability –equivalently the precise value of x at which one should switch from one to the other– have only been estimated on an empirical basis.

4.1. *Transverse momentum integrated yields*

The p_T -integrated multiplicity of charged particles is the most basic observable in particle collisions. For a variety of reasons though, it is also hard to compute with precision, unfortunately. To name a few: in practice, many computations of dN/dy rely on k_T -factorization, following the early papers by Kharzeev, Levin and Nardi^{55–57} who showed that it works surprising well to describe the centrality dependence of hadron production even in nucleus-nucleus collisions at RHIC energy, although it should not.^{58,59} In another approach, the multiplicity is computed numerically from an exact solution of the classical Yang-Mills equations, using a MV-model action with an energy dependent saturation momentum.⁶⁰ This accounts for multiple scattering both on the projectile and target side but assumes that the effective action far from the valence sources remains a local Gaussian. We expect, however, that these calculation will be improved in the foreseeable future to employ an effective action that solves JIMWLK. We review hadron multiplicities in A+A collisions in section 5.3.

The theoretical foundation for k_T -factorization is somewhat more solid in case of p+A collisions since dN/dy is dominated by $Q_{s,A} \gtrsim p_T \gtrsim Q_{s,p}$.⁶¹ Nevertheless some

hurdles remain, not the least of which is, of course, hadronization. All CGC based phenomenological computations of dN/dy assume that the p_T -integrated hadron yield is proportional to that of gluons. The number of hadrons per produced gluon could depend on energy, though.⁶² Furthermore, it is clear that the distribution of hadrons in rapidity need not be *identical* to that of gluons, especially when their density per unit of rapidity is high. More to the point: pseudo-rapidity distributions $dN/d\eta$ of unidentified charged hadrons involve a transformation from $y \rightarrow \eta$ which depends on the mass and p_T of a hadron; $\langle p_T \rangle$ increases with energy, with the mass numbers of projectile and target, and is affected by soft final-state interactions (at least in case of A+A collisions).

It is clear that computing $dN/d\eta$ distributions from first principles is a formidable problem. That said, with some level of optimism one may hope that the main dependence of $dN/d\eta$ on energy and system size is through the saturation scale Q_s . Indeed, one very important outcome of the p+A and A+A programs at RHIC and LHC, in terms of “soft” hadron multiplicities, is that this assumption works to a large degree. Thus, the *main* features of inclusive particle production *can* be understood within weakly-coupled, semi-hard (albeit non-linear) QCD although genuine non-perturbative effects such as hadronization physics or soft final-state interactions are obviously not entirely irrelevant.

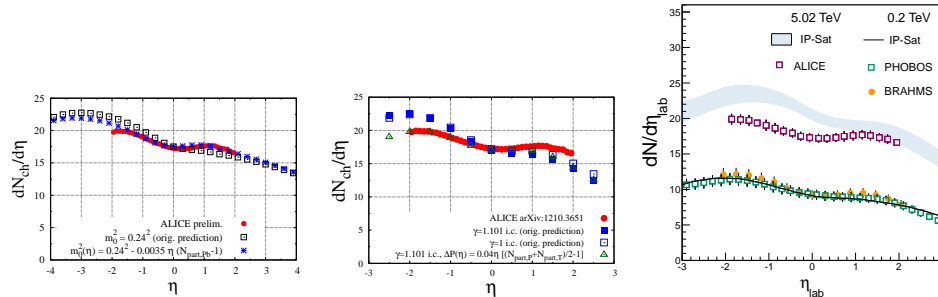


Fig. 2. Left: charged particle rapidity distribution for minimum-bias p+Pb collisions at 5 TeV from the KLN gluon saturation model.⁶³ Center: rcBK UGD.²⁸ Right: IP-Sat UGD.⁶⁴ ALICE data from ref.⁶⁵

We now proceed to show some of the most recent computations, within various implementations of the CGC formalism, of multiplicities in p+Pb collisions at LHC energies. We stress that all of these had been made public before the p+Pb pilot run at the LHC occurred in fall 2012^c. Fig. 2 shows the prediction of the KLN model⁶³ for 5 TeV. The original prediction depicted by open squares employed the exact same $y \rightarrow \eta$ transformation, specifically the same rapidity independent ratio of hadron

^cAlbeit, in most cases the initial predictions assumed a collision energy of $\sqrt{s} = 4.4$ TeV which was later updated to 5 TeV; also, initial predictions did not account for the rapidity shift by $\Delta y = \frac{1}{2} \log(82/208) \simeq -0.465$ of the experimental detectors towards the Pb beam and were updated later.

mass to transverse momentum $m/p_T = 0.24$, as for p+p collisions. At $\eta = 0$ the prediction essentially coincides with the data, in fact much better than its true level of accuracy. Away from midrapidity it exhibits a slightly steeper dependence on η than the data. At such level of detail, however, one can not discard hadronization effects entirely; this is illustrated in the figures by the “updated curve” (stars) which introduces a slight rapidity dependence of $m/\langle p_T \rangle$, with a sign that follows from the rapidity dependence of $\langle p_T \rangle \sim Q_{s,\text{Pb}}$.

A similar prediction from k_T -factorization with rcBK UGDs is shown in fig. 2 (center panel). Once again, $dN/d\eta$ at $\eta = 0$ matches the data at a level of a few percent but the η dependence predicted with the $y \rightarrow \eta$ transformation from p+p is somewhat too steep. A curve corresponding to rapidity dependent hadron transverse momentum $p_T = P + \Delta P(\eta)$ (open triangles) illustrates the sensitivity to detailed properties of the hadrons in the final state.

Yet another prediction for $dN/d\eta$ in p+Pb collisions employs k_T -factorization with UGDs from the IP-sat model.⁶⁴ An updated result for $\sqrt{s} = 5$ TeV, and including the above-mentioned rapidity shift, is shown again in fig. 2 on the right. These authors also provide uncertainty estimates shown by the bands. This prediction is also close to the data although it overpredicts the multiplicity at $\eta \lesssim 1$ somewhat. In part, this may be due to neglecting target thickness fluctuations which effectively suppress the multiplicity in the dense regime at $p_T < Q_s$ (see fig. 7 and related discussion in ref.²⁸).

Last but not least, Rezaeian provided another set of predictions for $\sqrt{s} = 4.4$ TeV in ref.⁶⁶ which is slightly higher than the above (again, without accounting for target thickness fluctuations). In all, it is quite remarkable that all of these implementations which differ in their hadronization prescription or in the treatment of the nuclear geometry and of Glauber fluctuations lead to similar predictions at $\eta = 0$ (deviations from the central value are $\pm 15\%$ or less); they all involved an extrapolation from d+Au collisions at RHIC by a good order of magnitude (factor of 25) in center-of-mass energy. This is consistent with expectations that the energy dependence of particle production is determined mainly by the growth of the gluon saturation scale rather than by genuinely non-perturbative soft physics.

4.2. *Single inclusive hadron yields and nuclear modification factors*

Nuclear effects on single particle production are typically evaluated in terms of ratios of particle yields called nuclear modification factors:

$$R_{pA}^h = \frac{dN^{pA \rightarrow hX}/dyd^2p_\perp}{N_{coll} dN^{pp \rightarrow hX}/dyd^2p_\perp}, \quad (9)$$

where N_{coll} is the number of binary nucleon-nucleon collisions in a p+A collision at a given energy. If high-energy nuclear reactions were a mere incoherent superposition of nucleon-nucleon collisions then the observed R_{pA} would equal unity. On the contrary, RHIC measurements in d+Au collisions^{67,68} show strong nuclear effects,

with mainly two opposite regimes: at mid rapidities the nuclear modification factors exhibit an enhancement in particle production at intermediate momenta $|p_\perp| \sim 2 \div 4$ GeV. In turn, a suppression at smaller momenta is observed. However, at forward rapidities the Cronin enhancement disappears, turning into an almost homogeneous suppression.

Single-hadron production data at mid-rapidity have been successfully analyzed through different formalisms and techniques, such as leading-twist perturbation theory, Glauber-eikonal multiple scatterings, or the Color Glass Condensate. These different approaches offer a comparably good description of the mid-rapidity RHIC data, so it is difficult to extract any clean conclusion about the physical origin of the Cronin enhancement. This is probably due to the kinematic region probed in these measurements. For a hadron momentum of $|p_\perp| \sim 2$ GeV, one is sensitive to $x \sim 0.01 \div 0.1$. In this region different physical mechanisms concur so that neither of the physical assumptions underlying the various approaches above is fully satisfied. Indeed, the coherence length, estimated to be $l_c \sim 1/(2m_N x) \sim 1 \div 10$ fm in the target rest frame is, on average, smaller than the nuclear diameter; hence the fully coherent treatment of the collision implicit in the CGC formalism is not completely justified and large- x corrections are expected to be relevant. Moreover, both the coherent or incoherent treatments of the collision need to invoke the presence of an intrinsic scale, presumably of non-perturbative origin, of the order of 1 GeV in order to reproduce the data, whose dynamical origin is not evident at all.

The situation at forward rapidities is better understood. Denoting p_\perp and y the transverse momentum and rapidity of the final state particles, the partons that can contribute to the cross section have a fraction of longitudinal momentum bounded from below by x_p (for partons from the proton wave function) and x_A (for partons from the nucleus wave function) given by

$$x_p = x_F, \quad x_A = x_F e^{-2y}. \quad (10)$$

Here we introduced the Feynman variable $x_F = |p_\perp| e^y / \sqrt{s_{NN}}$ with $\sqrt{s_{NN}}$ the collision energy per nucleon. Therefore with $\sqrt{s_{NN}} \gg |p_\perp|$ and forward rapidities $y > 0$, the process features $x_p \lesssim 1$ and $x_A \ll 1$, meaning that forward hadron production is sensitive only to high-momentum partons from the proton (well understood in QCD), while only small-momentum partons from the nucleus contribute. This is the ideal configuration for probing parton saturation effects, and indeed, saturation-based approaches were the only ones to correctly predict the suppression of forward particle production^{69,70} (as well as the azimuthal decorrelation of forward hadron pairs,⁷¹ described in the next sub-section).

After the forward-rapidity RHIC data confirmed the CGC expectations, it has been argued that the observed suppression of particle production at forward rapidities is not an effect associated to the small values of x_A probed in the nuclear wave function, but rather to energy-momentum conservation corrections relevant for $x_F \rightarrow 1$.^{72,73} Such corrections are not present in the CGC which relies on the eikonal approximation (this may explain why a K -factor is needed to describe

the suppression of very forward pions). The energy degradation of the projectile parton, neglected in the CGC, through either elastic scattering or induced gluon brehmsstrahlung would be larger for a nucleus than for a proton target, on account of the stronger color fields of the former, resulting in the relative suppression observed in data. LHC data are crucial to identify the correct suppression mechanism since LHC is able to probe small x_A while at the same time keeping x_F far from the kinematic limit so that energy-loss corrections should be negligible.

Before presenting theoretical predictions and comparisons to LHC data, let us discuss the kinematics in more detail. Contrary to popular belief, single-inclusive hadron production at mid-rapidity at the LHC does not probe the same values of x_A in the nucleus as forward hadron production at RHIC. The *minimal* values of x_A are indeed similar. However, the mean value is roughly given by $x_A/\langle z \rangle$, where $\langle z \rangle$ is the average momentum fraction carried by a final state hadron relative to its mother parton, due to the fragmentation process. At forward rapidity and RHIC energy, $\langle z \rangle$ is close to 1 but at mid-rapidity at the LHC it is around 0.3, meaning that larger values of x are probed there. In addition, for $p_t^{hadron} \sim Q_s$ one has $p_t^{parton} \sim Q_s/\langle z \rangle$, these two effects combine so that, for similar hadron transverse momenta, the suppression of R_{pA} should be less important at mid-rapidity at the LHC as compared to what has been measured at forward rapidities at RHIC.

For $1 < p_T < 3$ GeV, the transverse momentum range for which those data overlap, this is indeed what CGC calculations predict. This can be seen in the left panel of Fig. 3: the CGC predictions are around $R_{pPb} \sim 0.6 \div 0.9$, and within errors they agree with recent ALICE data. At higher p_T the CGC predictions are also confirmed but we emphasize that this would not have been the case without some recent development: the predictions of⁷⁸ for instance are well below the ALICE data. The main reason is that, in this latter study and in other earlier works, the impact-parameter dependence of the nuclear gluon density, and of the saturation scale, has not been described properly: minimum-bias predictions were obtained using an impact-parameter averaged saturation scale. Later CGC studies such as²⁸ have shown that it is very important to account for the proper nuclear geometry as well as for its attendant fluctuations.

Other theory comparisons with the ALICE mid-rapidity data show that, other than parton saturation effects, there are no cold matter effects. In particular there is no Cronin enhancement at low p_T and no suppression at high p_T . For $p_T > 4$ GeV, R_{pPb} is compatible with unity and well described by the leading-twist nuclear PDF approximation. Further data at backward rapidities, probing larger values of x_A , will be needed to confirm the anti-showing peak predicted in this approach. Conversely, additional data for forward rapidities, probing smaller values of x_A , will be needed to confirm the suppression pattern predicted in the CGC approach, as shown in the right panel of Fig. 3.

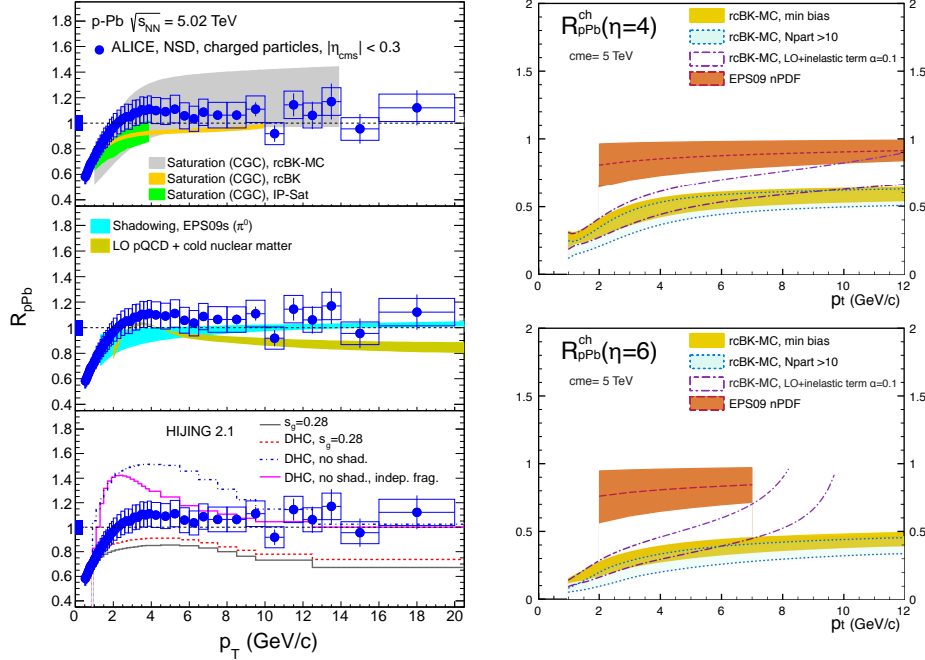


Fig. 3. Left: ALICE preliminary data⁷⁴ for the charged hadron nuclear modification factor at mid-rapidity as a function of p_T . The theoretical results correspond to the CGC calculations of,^{28,64,75} the nuclear PDF approach EPS09,⁴⁸ the cold-nuclear matter predictions of,⁷⁶ and the HIJING Monte Carlo.⁷⁷ Right: LO EPS09⁴⁸ and rcBK-MC²⁸ forward-rapidity predictions.

4.3. Double inclusive particle production and azimuthal correlations

We conclude this section on p+A collisions with a discussion of forward di-hadron correlations measured at RHIC (ridge-like correlations of rapidity separated di-hadrons measured at the LHC are discussed later in section 5.4). In the case of double-inclusive hadron production $pA \rightarrow h_1 h_2 X$, denoting $p_{1\perp}$, $p_{2\perp}$ and y_1 , y_2 the transverse momenta and rapidities of the final-state particles, the Feynman variables are $x_i = |p_{i\perp}| e^{y_i} / \sqrt{s_{NN}}$ and x_p and x_A read

$$x_p = x_1 + x_2, \quad x_A = x_1 e^{-2y_1} + x_2 e^{-2y_2}. \quad (11)$$

We shall only consider here the production of two forward particles, since this is the only case which is sensitive to values of x as small as in the single-inclusive case: $x_p \lesssim 1$ and $x_A \ll 1$. The central-forward measurement does not probe such kinematics: moving one particle forward increases significantly the value of x_p compared to the central-central case (for which $x_p = x_A = |p_{\perp}| / \sqrt{s_{NN}}$), but decreases x_A only marginally. In addition, we will focus on the $\Delta\phi$ dependence of the double-inclusive hadron spectrum, where $\Delta\phi$ is the difference between the azimuthal angles of the measured particles h_1 and h_2 .

The kinematic range for forward particle detection at RHIC is such that $x_p \sim 0.4$ and $x_A \sim 10^{-3}$. Therefore the dominant partonic subprocess is initiated by valence quarks in the proton and, at lowest order in α_s , the $pA \rightarrow h_1 h_2 X$ double-inclusive cross-section is obtained from the $qA \rightarrow qgX$ cross-section, the valence quark density in the proton $f_{q/p}$, and the appropriate hadron fragmentation functions $D_{h/q}$ and $D_{h/g}$:

$$\begin{aligned}
 dN^{pA \rightarrow h_1 h_2 X}(P, p_1, p_2) &= \int_{x_1}^1 dz_1 \int_{x_2}^1 dz_2 \int_{\frac{x_1}{z_1} + \frac{x_2}{z_2}}^1 dx f_{q/p}(x, \mu^2) \\
 &\times \left[dN^{qA \rightarrow qgX} \left(xP, \frac{p_1}{z_1}, \frac{p_2}{z_2} \right) D_{h_1/q}(z_1, \mu^2) D_{h_2/g}(z_2, \mu^2) + \right. \\
 &\left. dN^{qA \rightarrow qgX} \left(xP, \frac{p_2}{z_2}, \frac{p_1}{z_1} \right) D_{h_1/g}(z_1, \mu^2) D_{h_2/q}(z_2, \mu^2) \right] \quad (12)
 \end{aligned}$$

We have assumed independent fragmentation of the two final-state hadrons, therefore Eq. (12) cannot be used to compute the near-side peak around $\Delta\Phi = 0$. Doing so would require the use of poorly-known di-hadron fragmentation functions, rather we will focus on the away-side peak around $\Delta\Phi = \pi$ where saturation effects are important. Note also that if x_p would be smaller (this will be the case at the LHC), the gluon initiated processes $gA \rightarrow q\bar{q}X$ and $gA \rightarrow ggX$ should also be included in Eq. (12).

On the nucleus side, the gluon longitudinal momentum fraction varies between x_A and $e^{-2y_1} + e^{-2y_2}$. Therefore with large enough rapidities, only the small- x part of the nuclear wave function is relevant when calculating the $qA \rightarrow qgX$ cross section (there is no contamination from large x components). When probing the saturation regime, one expects $dN^{qA \rightarrow qgX}$ to be a non-linear function of the nuclear gluon distribution, i.e. that this cross section cannot be factorized further: $dN^{qA \rightarrow qgX} \neq f_{g/A} \otimes dN^{qg \rightarrow qgX}$. Using the CGC approach to describe the small- x part of the nucleus wave function, the $qA \rightarrow qgX$ cross section was calculated in,^{71, 79–81} and indeed it was found that, due to the fact that small- x gluons in the nuclear wave function behave coherently and not individually, the nucleus cannot be described by only a single-gluon distribution.

The $qA \rightarrow qgX$ cross section is instead expressed in terms of correlators of Wilson lines (which account for multiple scatterings), with up to a six-point correlator averaged over the CGC wave function. At the moment, it is practically difficult to evaluate the six-point function. In the large- N_c limit, it factorizes into a dipole scattering amplitude times a trace of four Wilson lines (or quadrupole), and the latter can in principle be obtained by solving an evolution equation written down in.⁷⁹ However, this implies a significant amount of numerical work, and also requires to introduce an unknown initial condition. In practice, further approximations have been used, and this is where different phenomenological studies of forward di-hadron correlations in p+A collisions differ:

- in Ref.,⁸² the quadrupole is simply disregarded, the cross-section is obtained

- solely from the dipole amplitude, using the so-called k_T -factorized formula recovered in the limit $Q_s/|p_{\perp 1,2}| \ll 1$. Saturation effects are nevertheless included in the UDGs, and it is done using the GBW parametrization.⁴⁰
- in Ref.,⁸³ the quadrupole is evaluated using the so-called Gaussian approximation of B-JIMWLK evolution, however only the *elastic* contribution is kept. The non-linear evolution is obtained using the rcBK equation.
 - in Ref.,⁸⁴ the complete Gaussian expression of the quadrupole is used, however only the so-called correlation limit $Q_s \sim |p_{\perp 1} + p_{\perp 2}| \ll |p_{\perp 1,2}|$ is considered. Saturation effects are included using the GBW parametrization. The gluon-initiated processes calculated in²⁹ are included for the first time.
 - in Ref.,³⁴ the complete Gaussian expression of the quadrupole is used, and the non-linear evolution is obtained using the rcBK equation. Gluon-initiated processes are not included.

We now come to the comparison with data. Nuclear effects on di-hadron correlations are typically evaluated in terms of the coincidence probability to, given a trigger particle in a certain momentum range, produce an associated particle in another momentum range. The coincidence probability is given by $CP(\Delta\phi) = N_{pair}(\Delta\phi)/N_{trig}$ with

$$N_{pair}(\Delta\phi) = \int_{y_i, |p_{i\perp}|} \frac{dN^{pA \rightarrow h_1 h_2 X}}{d^3p_1 d^3p_2}, \quad N_{trig} = \int_{y, p_\perp} \frac{dN^{pA \rightarrow h X}}{d^3p}. \quad (13)$$

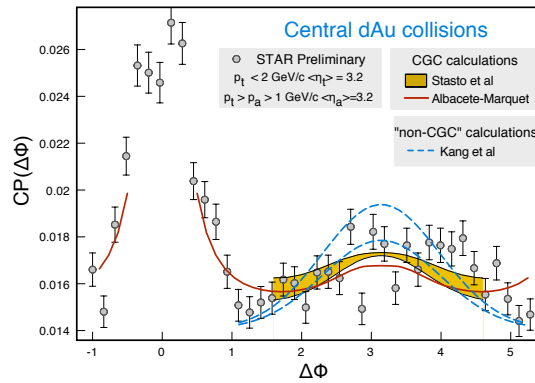


Fig. 4. STAR preliminary data⁸⁵ for the Coincident Probability between pairs of hadrons as a function of the relative azimuthal angle in d+Au collisions at RHIC. The theoretical results correspond to two CGC-based calculations⁸³ and⁸⁴ and a *higher-twist* one.⁸⁶ Figure from⁸⁷

The STAR data for the coincidence probability obtained with two neutral pions are displayed in Fig. 4 for central d+Au collisions. The nuclear modification of the di-pion azimuthal correlation is quite impressive, considering that the prominent away-side peak seen in p+p collisions is absent in central d+Au collisions, in agree-

ment with the behavior first predicted in.⁷¹ The data are compared with the CGC calculations of⁸³ and,⁸⁴ as well as with a non-CGC approach discussed below. As mentioned before, the complete near-side peak is not computed, as Eq. (12) does not apply around $\Delta\phi = 0$. Note also that, since uncorrelated background has not been extracted from the data, the overall normalization of the theory points has been adjusted by adding a constant shift.

The physics of the disappearance of the away-side peak is the following. The two measured hadrons predominantly come from a quark and a gluon, which were back-to-back while part of the initiating valence quark wave function. During the interaction, if they are put on shell by a single parton from the target carrying zero transverse momentum, as is the case when non-linear effects are not important, then the hadrons are emitted back-to-back (up to a possible transverse momentum broadening during the fragmentation process). By contrast, in the saturation regime, the quark and antiquark receive a coherent transverse momentum kick whose magnitude is of order Q_s , which depletes the correlation function around $\Delta\phi = \pi$, for hadron momenta not much higher than Q_s .

The sizable width of the away-side peak in Fig. 4 cannot be described within the leading-twist collinear factorization framework, which completely neglects non-linear effects. While it may not be obvious from single-inclusive measurements, this indicates that power corrections are important when $|p_\perp| \sim 2$ GeV. At such low transverse momenta, collinear factorization does not provide a good description of particle production in p+A collisions. In contrast, CGC calculations which do incorporate non-linear effects by resumming power corrections can reproduce the suppression phenomenon. Ref.⁸⁶ uses a non-CGC framework where only the first power corrections to leading-twist collinear factorization are considered.

5. Bulk features of multiparticle production in A+A, p+A and p+p collisions

5.1. Multiplicity distributions in p+p and p+A collisions

In recent years calculations of single-inclusive multiplicities within the CGC framework have been extended to *multiplicity distributions* and to their evolution with energy and system size. Much of this initial progress on multiparticle production in the non-linear regime is based on the framework of classical fields. Some basic insight into quantum evolution effects on various moments of the multiplicity distributions has also been developed⁸⁸ but an explicit discussion of their properties is still lacking.

Assuming dominance of classical fields, the probability to produce q particles is given by⁸⁹

$$\left\langle \frac{d^q N}{dy_1 \cdots dy_q} \right\rangle_{\text{conn.}} = C_q \left\langle \frac{dN}{dy_1} \right\rangle \cdots \left\langle \frac{dN}{dy_q} \right\rangle \quad (14)$$

with the reduced moments

$$C_q = \frac{(q-1)!}{k^{q-1}}. \quad (15)$$

This expression is valid with logarithmic accuracy and was derived under the assumption that all transverse momentum integrals over $p_{T,1} \cdots p_{T,q}$ are effectively cut off in the infrared at the non-linear scale.

The fluctuation parameter k in eq. (15) is of order

$$k \sim (N_c^2 - 1) Q_s^2 S_\perp. \quad (16)$$

The numerical prefactor (in the classical approximation) has been determined by a numerical computation to all orders in the valence charge density in ref.⁹⁰

The multiplicity distribution is therefore approximately a negative binomial distribution (NBD),⁸⁹

$$P(n) = \frac{\Gamma(k+n)}{\Gamma(k)\Gamma(n+1)} \frac{\bar{n}^n k^k}{(\bar{n}+k)^{n+k}}. \quad (17)$$

Indeed, multiplicity distributions observed in high-energy p+p collisions (in the central region) can be described reasonably well by a NBD, see for example refs.^{64,91} The parameter k^{-1} determines the variance of the distribution^d and can be obtained from the (inclusive) double-gluon multiplicity:

$$\left\langle \frac{d^2N}{dy_1 dy_2} \right\rangle_{\text{conn.}} = \frac{1}{k} \left\langle \frac{dN}{dy_1} \right\rangle \left\langle \frac{dN}{dy_2} \right\rangle. \quad (18)$$

This expression shows that the perturbative expansion of k^{-1} starts at $\mathcal{O}(\alpha_s^0)$ since the connected diagrams on the l.h.s. of eq. (18) involve the same number of sources and vertices as the disconnected diagrams on the r.h.s. of that equation.⁹² Since the *mean* multiplicity in the classical limit is of order $\bar{n} \equiv \langle dN/dy \rangle \sim 1/\alpha_s$ it follows that $\bar{n}/k \sim 1/\alpha_s \gg 1$. This, in fact, corresponds to the limit where the NBD multiplicity distributions exhibit KNO scaling.⁹³ The semi-classical strong-field limit of a Gaussian effective theory relates the emergence of KNO scaling in p_\perp -integrated multiplicity distributions to properties of small- x gluons around the saturation scale.⁹²

KNO scaling conjectures that the particle multiplicity distribution in high-energy hadronic collisions is *universal* (i.e., energy independent) if expressed in terms of the fractional multiplicity $z \equiv n/\bar{n}$. This is satisfied in first approximation in the central (pseudo-) rapidity region at energies ≥ 200 GeV as shown in fig. 5. For a detailed review of pre-LHC data see ref.⁹⁷

However, more precise NBD fits to the multiplicity distributions reveal that \bar{n}/k increases somewhat with energy, and so KNO scaling is not exact. An increase of $\bar{n}/k \sim 1/\alpha_s$ with energy may be partially explained by running of the coupling

^dThe width is given by $\bar{n} \sqrt{k^{-1} + \bar{n}^{-1}} \sim \bar{n}/\sqrt{k}$ where the latter approximation applies in the limit $\bar{n}/k \gg 1$.

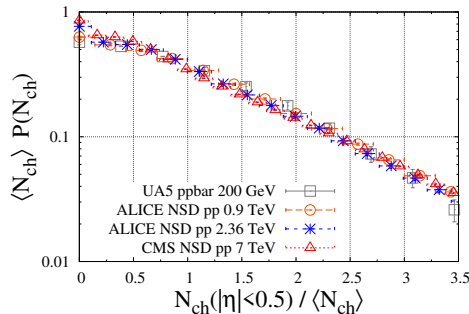


Fig. 5. KNO scaling plot of charged particle multiplicity distributions in non-single diffractive $pp/p\bar{p}$ collisions at various energies as measured by the UA5,⁹⁴ ALICE⁹⁵ and CMS⁹⁶ collaborations, respectively. Note that we restrict to the central rapidity region $|\eta| < 0.5$ and to the bulk of the distributions up to 3.5 times the mean multiplicity.

with $Q_s(x)$ but this goes beyond the classical approximation. Corrections beyond the classical limit are also indicated by the fact that at lower energies higher-order factorial moments G_q of the distribution are significantly different from the reduced moments C_q .⁹⁸

$$G_q \equiv \frac{\langle n(n-1)\cdots(n-q+1) \rangle}{\bar{n}^q}, \quad C_q \equiv \frac{\langle n^q \rangle}{\bar{n}^q}. \quad (19)$$

Note that the difference of G_q and C_q is subleading in the density of valence charges ρ . In fact, while eq. (15) has been derived for a quadratic MV-model action which applies near infinite density, at finite density the action contains additional terms $\sim \rho^4$.^{23,99} These operators provide corrections to the moments of the multiplicity distribution.⁹²

Finally we also point out that approximate KNO scaling has been predicted to persist even for min-bias p+Pb collisions at LHC energies,⁹¹ with deviations from the KNO curve from p+p collisions at a level of “only” $\sim 25\%$. This is in spite of Glauber fluctuations of the number of target participants which of course exist for a heavy-ion target. The multiplicity distribution in p+A collisions thus tests the expectation that intrinsic particle production fluctuations are dominated by the dilute source, i.e. that $k \sim \min(T_A, T_B)$ is proportional to the thickness of the more dilute collision partner. Furthermore, it can provide valuable constraints for models of initial-state fluctuations in A+A collisions which are currently of great interest (see section 5.2).

5.2. The initial state in A+A collisions

The CGC formalism also offers a framework which allows one to determine the initial state of a heavy-ion collision. This refers to the distribution of produced particles in momentum as well as transverse coordinate space which determines the initial condition for the subsequent thermalization stage, followed by (viscous)

hydrodynamics. Understanding the thermalization process in high-energy heavy-ion collisions is a topic which is currently under intense investigation; we refer the interested reader to a recent review by F. Gelis published in this journal.³⁹

In practice, the “detailed” dynamics of thermalization is often skipped and the p_T -integrated distribution of produced particles in the transverse plane is used directly to initialize hydrodynamic simulations. This appears reasonable if one is interested mainly in the features of dN/dyd^2r_T over length scales larger than the thermalization time τ_{th} . On the other hand, density fluctuations on shorter scales could be washed out, see e.g. ref.⁶⁰ for a concrete example applying classical Yang-Mills field dynamics.

Instead of resorting to the CGC formalism a much simpler shortcut to the initial dN/dyd^2r_T is to assume that the local density of particles produced at a point r_T is simply proportional to the average density of projectile and target participants, $dN/dyd^2r_T \sim (\rho_{\text{part}}^A(r_T) + \rho_{\text{part}}^B(r_T))/2$. This “wounded nucleon” model, often times also labeled “Glauber model”, clearly must capture the rough features of dN/dyd^2r_T . On the other hand, it is evident from the increase of $(1/N_{\text{part}}) dN/d\eta$ or $(1/N_{\text{part}}) dE_T/d\eta$ from peripheral to central Pb+Pb collisions by about a factor of two (see fig.7) that such a model is far from accurate. There is no reason to believe that the second harmonic moment of the density distribution in the transverse plane, the so-called eccentricity $\varepsilon = \langle y^2 - x^2 \rangle / \langle y^2 + x^2 \rangle$ would do better (the same goes for higher moments). Indeed, a variety of CGC models which do describe the centrality dependence of dN/dy predict higher eccentricity ε than the “wounded nucleon model”.^{49, 60, 100–102}

The “wounded nucleon model” for soft particle production can be improved by adding a semi-hard component. It has to incorporate impact parameter and Q^2 dependent shadowing in order to smoothly interpolate to p+p collisions in very peripheral collisions and to $\sim N_{\text{coll}}$ scaling at high p_T ;⁴⁸ also, the energy dependence of the low- p_T cutoff required by leading-twist calculations needs to be fixed carefully to reproduce measured multiplicities.

The initial spatial particle distribution exhibits large fluctuations. They manifest in non-zero elliptic flow v_2 in central heavy-ion collisions¹⁰³ as well as in a large “triangular flow” component v_3 .¹⁰⁴ One source of fluctuations is due to the locations of participant nucleons;¹⁰³ these have also been incorporated early on in Monte-Carlo implementations of the k_T -factorization formula with KLN UGDs.^{49, 50}

However, even for a fixed (local) number of participants there are intrinsic particle production fluctuations. This is most evident from the wide multiplicity distribution in non-single diffractive p+p collisions (see section 5.1). A suitable extrapolation to A+A collisions has to be included both in “wounded nucleon”¹⁰⁵ as well as in CGC based⁹¹ Monte-Carlo models. In the CGC approach, intrinsic particle production fluctuations are expected to occur on sub-nucleon distance scales on the order of $\sim 1/Q_s$,³⁵ as shown in fig. 6. It is interesting to note that early CGC initial state models which do *not* incorporate intrinsic particle production fluctuations^{49, 50} appear to be inconsistent with the distributions of angular flow harmonics measured

by the ATLAS collaboration¹⁰⁶ while recent approaches can describe higher eccentricity harmonics rather well.¹⁰⁷ The “cosmology of heavy-ion collisions” will be to

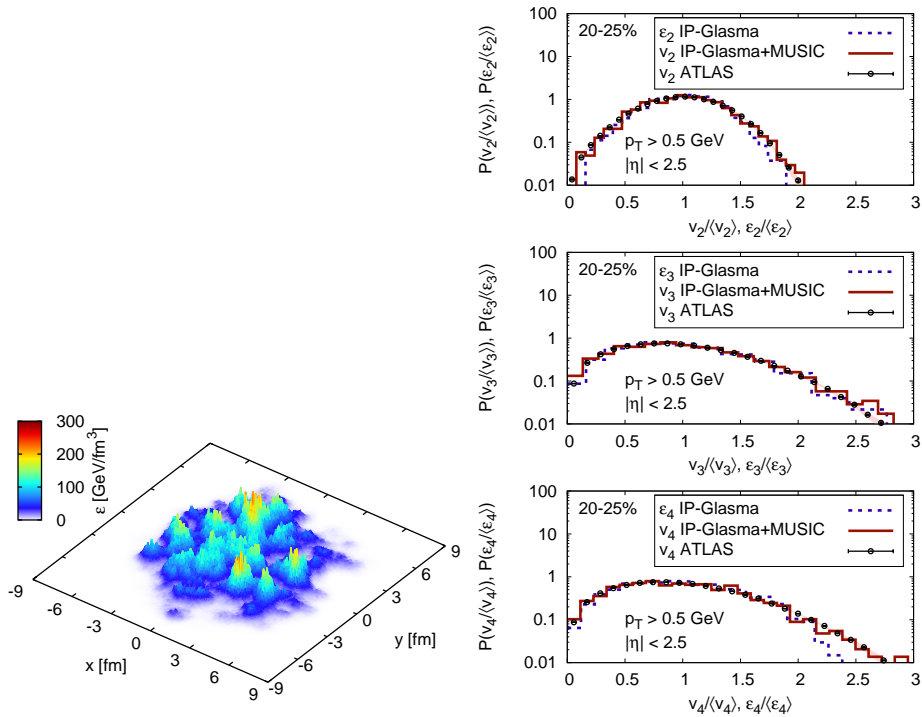


Fig. 6. Left: fluctuating energy density distribution at midrapidity and time $\tau = 0.2$ fm/c in an A+A collision.³⁵ Right: Scaled distributions of various azimuthal harmonics for Pb+Pb collisions at 2.76 TeV (20%-25% centrality class) from the CGC implementation of ref.¹⁰⁷ compared to ATLAS data.

understand the nature, scale, magnitude and evolution of these fundamental QCD fluctuations in detail. It represents a very exciting avenue for future research.

5.3. Multiplicities and transverse energy

We now turn to the centrality dependence of the multiplicity and transverse energy in heavy-ion collisions at LHC energies as obtained from k_T -factorization with rcBK UGDs. We recall that k_T -factorization is not expected to provide accurate results for p_T integrated observables in A+A collisions.^{58, 59} Furthermore, we restrict to the initial “gluon liberation” process and do not account for subsequent gluon multiplication towards thermalization.^{58, 59, 108} Nevertheless, it is of course important to check that basic trends such as the centrality dependence of dN/dy are consistent with theoretical expectations regarding the dependence of the saturation

momentum on the thickness of a nucleus.^{57,109}

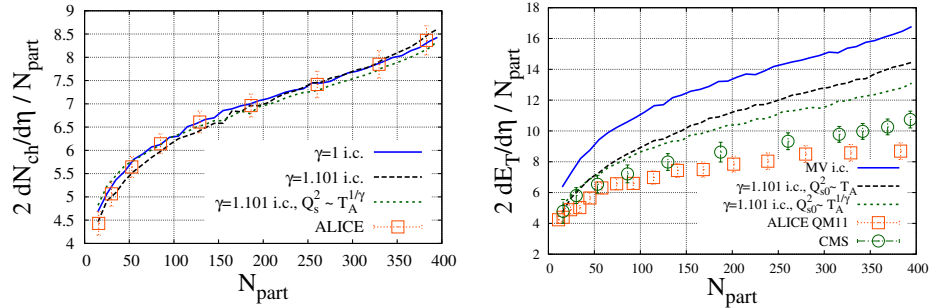


Fig. 7. Left: Centrality dependence of the charged particle multiplicity at midrapidity, $\eta = 0$; Pb+Pb collisions at 2760 GeV. We compare our calculation for two UGDs to data by the ALICE collaboration. Right: Centrality dependence of the transverse energy at $\eta = 0$.

We shall focus on the centrality dependence of the charged particle multiplicity at central rapidity, $\eta = 0$, which we determine along the lines described at the beginning of section 4. The result is shown in Fig. 7 for the UGDs with MV-model ($\gamma = 1$) and AAMQS ($\gamma = 1.101$ and $Q_s^2(x_0) \sim T_A$ or $Q_s^2(x_0) \sim T_A^{1/\gamma}$) initial conditions. We use $K = 1.43$ for the former and $K = 2.0, 2.3$ for the latter. The number of final hadrons per gluon is $\kappa_g = 5$ in all three cases.

Aside from normalization factors, all UGDs give a rather similar centrality dependence of the multiplicity, and are in good agreement with ALICE data.^{110,111} On the other hand, they differ somewhat in their prediction for the transverse energy. This is of course due to the fact that the $\gamma > 1$ initial condition suppresses the high- k_t tail of the UGD^e. With the K -factors mentioned above these UGDs match the measured E_t in peripheral collisions. This is a sensible result since one does not expect large final-state effects in very peripheral collisions. For the most central collisions the energy deposited initially at central rapidity is about 0.5% of the energy of the beams and exceeds the preliminary measurements by ALICE¹¹² and CMS¹¹³ by roughly 50%. This leaves room for $-p \Delta V$ work performed by longitudinal hydrodynamic expansion.¹¹⁴⁻¹¹⁶

5.4. The CGC and its ridge

In this section we discuss briefly the “ridge” structure observed in heavy-ion collisions at RHIC and in high-multiplicity p+p and p+Pb collisions at the LHC. A review dedicated entirely to this phenomenon has appeared recently in ref.¹¹⁷

^eOne should keep in mind though that our estimate of the initial transverse energy carries a significant uncertainty of at least $\pm 15\%$ related to our choice of K -factor; it is *not* determined accurately by the multiplicity since the latter involves only the product of K -factor and gluon \rightarrow hadron multiplication factor κ_g .

The “ridge” refers to two-particle correlations at *small* relative azimuth, $\Delta\phi \sim 0$, which extends over at least several units of relative (pseudo-)rapidity $\Delta\eta$, perhaps even all the way to the sources. These do not correspond to particles produced in a binary collision since those would appear in opposite azimuthal hemispheres, due to transverse momentum conservation.

What makes the ridge particularly interesting is that particles separated by a large pseudorapidity interval $\Delta\eta$ are causally disconnected and hence can not be correlated, unless they were produced early on at a time on the order of $\tau \sim \tau_f \exp(-\Delta\eta/2)$ or less.¹¹⁸ This argument relies on the assumption of Bjorken longitudinal boost invariance.

The ridge has been first observed in Au+Au collisions at RHIC.^{119–121} The “heavy-ion ridge” is difficult to interpret from a CGC perspective since both the amplitude as well as the azimuthal collimation of the correlation are certainly modified by final-state interactions with the dense medium; those might be interpreted as jet-medium interactions, hydrodynamic flow etc.

The discovery by CMS of similar ridge correlations in high multiplicity p+p collisions at 7 TeV therefore represented a major breakthrough. The duration of any final-state interactions for such small systems (in the transverse direction) clearly must be much shorter than in heavy-ion collisions: hydrodynamics predicts that (energy) density gradients decay on a time scale $\sim R/c_S$ where $c_s \simeq 1/\sqrt{3}$ denotes the relativistic speed of sound^f. On the other hand, within the CGC framework it is only the local density of gluons that matters but not the size and life-time of the system; the ridge correlation is explained as an initial-state effect, anyhow.

CMS has recently confirmed such ridge correlations also for high-multiplicity p+Pb collisions at 5 TeV as shown in fig. 8. While the radial extent of the collision zone and the particle density is comparable to that from high-multiplicity p+p collisions the observed amplitude of the ridge is much higher. One may anticipate that this should be related to the fact that multiplicity fluctuations in p+Pb are helped by the presence of Glauber fluctuations of N_{part} ;¹²⁵ we shall return to this point below.

The origin of the correlation can then be explained in two ways. In the Kovner-Lublinsky picture^{117, 126, 127} two incoming gluons from the projectile wave function with different rapidities scatter off the dense target field. If their relative impact parameter is less than the correlation length $1/Q_{s,T}$ of the dense gluons in the target, and if their color charges are alike, they prefer to scatter to a relative azimuthal angle $\Delta\phi \sim 0$ and lead to a “near side” ridge. Projectile gluons with opposite color charges, a configuration which is equally likely to occur, on the other hand prefer to scatter to $\Delta \sim \pi$. Ref.¹¹⁷ makes the interesting prediction that this “degeneracy” of the near-side and away-side ridges is lifted in case of projectile quarks; this could in

^fHere, R denotes the scale of gradients which may even be substantially smaller than the overall radial extent of the collision zone. However, the radial expansion of very small density spikes is damped by viscosity.

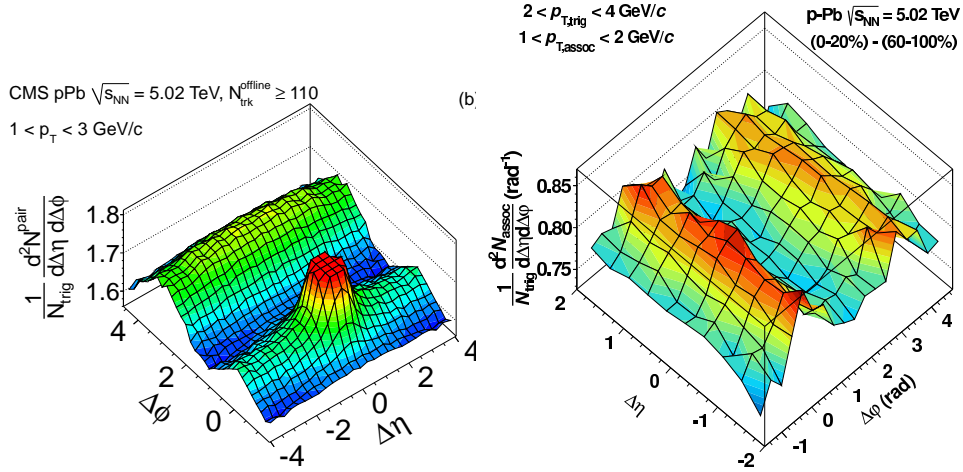


Fig. 8. Left: the ridge in high-multiplicity p+Pb collisions at 5 TeV as seen by CMS;¹²² particles with $1 \text{ GeV} \leq p_T \leq 3 \text{ GeV}$. Right: ALICE ridge with *subtracted* jet yield reveal the dipole correlation.¹²³ ATLAS results for the p+Pb ridge are presented in ref.¹²⁴

principle be tested if one could trigger on hadrons which are more likely to originate from quark fragmentation.

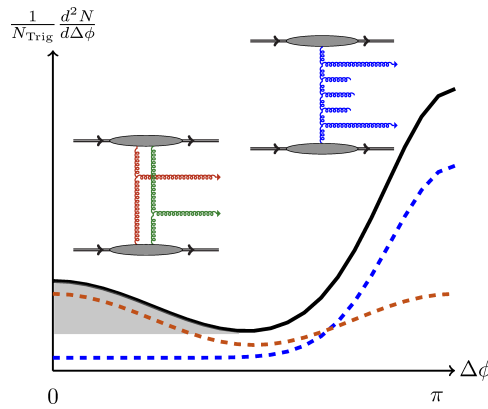


Fig. 9. Illustration of the diagrams that dominate at different $\Delta\phi$.¹²⁵

Another underlying picture for correlated production is as follows (see illustration in fig. 9). Two hard gluons from the same ladder are nearly back to back, by conservation of transverse momentum. On the other hand, those produced in separate ladders can have any relative angle. For correlated production, however, the two ladders need to be connected through the sources after squaring the amplitude. This is achieved by flipping the sources of the two ladders in the amplitude and its c.c.;

the resulting diagrams are enhanced if the density of sources is non-perturbatively high.¹¹⁸ In fact, this leads to a variety of contributions (incl. HBT-like correlations) as discussed in more detail in ref.¹²⁸ It has been realized early on that the “ridge” correlations are actually not uniform in $\Delta\phi$ but that the relative angle peaks at $\Delta\phi \sim 0$ and $\Delta\phi \sim \pi$.^{129–131}

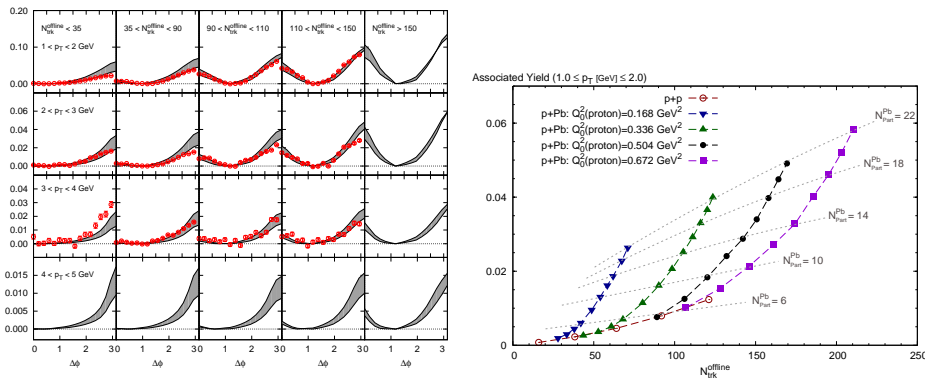


Fig. 10. Left: correlated particle yield after ZYAM subtraction as a function of relative azimuth in different centrality bins. Right: associated near-side yield as a function of multiplicity $N_{\text{trk}}^{\text{offline}}$: dashed curves / symbols show how the yield increases with the number of participants in the Pb target, thin dotted lines track its dependence on the valence charge density in the proton. Both figures from ref.¹²⁵

The current state of the art *quantitative* results are due to Dusling and Venugopalan.^{125,132} They describe not only the small-angle but also the back to back correlations and in fact the entire “matrix” of correlations as a function of the transverse momenta of trigger and associated particle, and for different bins of multiplicity (the latter shown fig. 10, left). We do not delve into details here but do return to a point mentioned above. Fig. 10, right, shows how the associated yield increases with the overall multiplicity $N_{\text{trk}}^{\text{offline}}$. For p+p collisions a very high multiplicity is due to rare extreme density fluctuations in either of the nucleons; in p+Pb collisions high multiplicity fluctuations are helped by the presence of additional Glauber fluctuations of the target thickness. Folding the two, ref.¹²⁵ obtains a very natural explanation for the increased near-side yield in p+Pb as compared to p+p at the same multiplicity $N_{\text{trk}}^{\text{offline}}$.

6. Conclusions

Fourty years after the discovery of QCD, it is an established fact today that the density of gluons in a hadron grows rapidly with rapidity. Present day colliders have the potential to make us understand at what light-cone momenta and transverse distance or momentum scales non-linear color field interactions set in. Collisions

with large heavy-ion targets are the most promising environment for this physics. We hope we could shed some light in this review on the prospects of present p+A, A+A and possible future e+A programs to answer some related fundamental questions in QCD. The so-called “Color Glass Condensate” formalism to high-density QCD provides a systematic framework to address many of the underlying phenomena in a consistent way. Nevertheless, at present phenomenological applications often differ in terms of implementation and involve various approximations. Quantitative comparisons to data are therefore crucial in order to test the accuracy of our current tools such as BK evolution in the running-coupling approximation. The forthcoming p+Pb run at the LHC will advance tremendously our understanding of high-energy interactions and of the initial state of heavy-ion collisions.

Acknowledgments

The work of J. L. Albacete is supported by a fellowship from the Théorie LHC France initiative funded by the IN2P3. A.D. is supported by the DOE Office of Nuclear Physics through Grant No. DE-FG02-09ER41620 and by The City University of New York through the PSC-CUNY Research Award Program, grant 65041-0043.

References

1. L. V. Gribov, E. M. Levin and M. G. Ryskin, *Phys. Rept.* **100**, 1 (1983).
2. A. H. Mueller and J.-w. Qiu, *Nucl. Phys.* **B268**, 427 (1986).
3. L. D. McLerran and R. Venugopalan, *Phys. Rev.* **D49**, 2233 (1994), [hep-ph/9309289](#).
4. L. D. McLerran and R. Venugopalan, *Phys. Rev.* **D49**, 3352 (1994), [hep-ph/9311205](#).
5. Y. V. Kovchegov, *Phys. Rev.* **D54**, 5463 (1996), [hep-ph/9605446](#).
6. I. Balitsky, *Nucl. Phys.* **B463**, 99 (1996), [hep-ph/9509348](#).
7. J. Jalilian-Marian, A. Kovner, A. Leonidov and H. Weigert, *Phys. Rev.* **D59**, 014014 (1998), [hep-ph/9706377](#).
8. J. Jalilian-Marian, A. Kovner and H. Weigert, *Phys. Rev.* **D59**, 014015 (1998), [hep-ph/9709432](#).
9. A. Kovner, J. G. Milhano and H. Weigert, *Phys. Rev.* **D62**, 114005 (2000), [hep-ph/0004014](#).
10. E. Iancu, A. Leonidov and L. D. McLerran, *Nucl. Phys.* **A692**, 583 (2001), [hep-ph/0011241](#).
11. E. Ferreiro, E. Iancu, A. Leonidov and L. McLerran, *Nucl. Phys.* **A703**, 489 (2002), [hep-ph/0109115](#).
12. I. Balitsky, *Nucl. Phys.* **B463**, 99 (1996), [arXiv:hep-ph/9509348 \[hep-ph\]](#).
13. Y. V. Kovchegov, *Phys. Rev.* **D60**, 034008 (1999), [hep-ph/9901281](#).
14. X.-N. Wang and M. Gyulassy, *Phys. Rev.* **D44**, 3501 (1991).
15. I. Lokhtin, L. Malinina, S. Petrushanko, A. Snigirev, I. Arsene *et al.*, *Comput. Phys. Commun.* **180**, 779 (2009), [arXiv:0809.2708 \[hep-ph\]](#).
16. N. Armesto, (ed.) *et al.*, *J. Phys.* **G35**, 054001 (2008), [arXiv:0711.0974 \[hep-ph\]](#).
17. I. Balitsky and G. A. Chirilli, *Phys. Rev.* **D77**, 014019 (2008), [arXiv:0710.4330 \[hep-ph\]](#).
18. Y. Kovchegov and H. Weigert, *Nucl. Phys.* **A 784**, 188 (2007), [hep-ph/0609090](#).
19. I. I. Balitsky, *Phys. Rev. D* **75**, 014001 (2007), [hep-ph/0609105](#).

20. J. L. Albacete and Y. V. Kovchegov, *Phys. Rev.* **D75**, 125021 (2007), [arXiv:0704.0612 \[hep-ph\]](#).
21. G. Beuf, *Phys.Rev.* **D85**, 034039 (2012), [arXiv:1112.4501 \[hep-ph\]](#).
22. I. Balitsky and G. A. Chirilli, *Phys.Rev.* **D83**, 031502 (2011), [arXiv:1009.4729 \[hep-ph\]](#).
23. A. Dumitru and E. Petreska, *Nucl.Phys.* **A879**, 59 (2012), [arXiv:1112.4760 \[hep-ph\]](#).
24. W. Horowitz and Y. V. Kovchegov, *Nucl.Phys.* **A849**, 72 (2011), [arXiv:1009.0545 \[hep-ph\]](#).
25. G. A. Chirilli, B.-W. Xiao and F. Yuan, *Phys.Rev.Lett.* **108**, 122301 (2012), [arXiv:1112.1061 \[hep-ph\]](#).
26. T. Altinoluk and A. Kovner, *Phys.Rev.* **D83**, 105004 (2011), [arXiv:1102.5327 \[hep-ph\]](#).
27. J. Jalilian-Marian and A. H. Rezaeian, *Phys.Rev.* **D85**, 014017 (2012), [arXiv:1110.2810 \[hep-ph\]](#).
28. J. L. Albacete, A. Dumitru, H. Fujii and Y. Nara, *Nucl.Phys.* **A897**, 1 (2013), [arXiv:1209.2001 \[hep-ph\]](#).
29. F. Dominguez, C. Marquet, B.-W. Xiao and F. Yuan, *Phys.Rev.* **D83**, 105005 (2011), [arXiv:1101.0715 \[hep-ph\]](#).
30. H. Fujii, F. Gelis and R. Venugopalan, *Nucl.Phys.* **A780**, 146 (2006), [arXiv:hep-ph/0603099 \[hep-ph\]](#).
31. Y. V. Kovchegov, J. Kuokkanen, K. Rummukainen and H. Weigert, *Nucl.Phys.* **A823**, 47 (2009), [arXiv:0812.3238 \[hep-ph\]](#).
32. C. Marquet and H. Weigert, *Nucl.Phys.* **A843**, 68 (2010), [arXiv:1003.0813 \[hep-ph\]](#).
33. E. Iancu and D. Triantafyllopoulos, *JHEP* **1111**, 105 (2011), [arXiv:1109.0302 \[hep-ph\]](#).
34. T. Lappi and H. Mantysaari (2012), [arXiv:1209.2853 \[hep-ph\]](#).
35. B. Schenke, P. Tribedy and R. Venugopalan, *Phys.Rev.Lett.* **108**, 252301 (2012), [arXiv:1202.6646 \[nucl-th\]](#).
36. F. Gelis, T. Lappi and R. Venugopalan, *Phys.Rev.* **D78**, 054020 (2008), [arXiv:0807.1306 \[hep-ph\]](#).
37. F. Gelis, T. Lappi and R. Venugopalan, *Phys. Rev.* **D78**, 054019 (2008), [arXiv:0804.2630 \[hep-ph\]](#).
38. K. Dusling, T. Epelbaum, F. Gelis and R. Venugopalan, *Nucl.Phys.* **A850**, 69 (2011), [arXiv:1009.4363 \[hep-ph\]](#).
39. F. Gelis (2012), [arXiv:1211.3327 \[hep-ph\]](#).
40. K. Golec-Biernat and M. Wüsthoff, *Phys. Rev.* **D59**, 014017 (1998), [hep-ph/9807513](#).
41. D. N. Triantafyllopoulos, *Nucl. Phys.* **B648**, 293 (2003), [hep-ph/0209121](#).
42. E. Iancu, K. Itakura and S. Munier, *Phys. Lett.* **B590**, 199 (2004), [hep-ph/0310338](#).
43. H. Kowalski and D. Teaney, *Phys. Rev.* **D68**, 114005 (2003), [hep-ph/0304189](#).
44. A. H. Rezaeian, M. Siddikov, M. Van de Klundert and R. Venugopalan (2012), [arXiv:1212.2974 \[hep-ph\]](#).
45. J. L. Albacete, N. Armesto, J. G. Milhano and C. A. Salgado, *Phys. Rev.* **D80**, 034031 (2009), [arXiv:0902.1112 \[hep-ph\]](#).
46. J. L. Albacete, N. Armesto, J. G. Milhano, P. Quiroga Arias and C. A. Salgado, *Eur.Phys.J.* **C71**, 1705 (2011), [arXiv:1012.4408 \[hep-ph\]](#), * Temporary entry *.
47. H. Fujii, K. Itakura, Y. Kitadono and Y. Nara, *J.Phys.G* **G38**, 124125 (2011), [arXiv:1107.1333 \[hep-ph\]](#).
48. I. Helenius, K. J. Eskola, H. Honkanen and C. A. Salgado, *JHEP* **1207**, 073 (2012),

- arXiv:1205.5359 [hep-ph].
49. H.-J. Drescher and Y. Nara, *Phys.Rev.* **C75**, 034905 (2007), arXiv:nucl-th/0611017 [nucl-th].
 50. H.-J. Drescher and Y. Nara, *Phys. Rev.* **C76**, 041903 (2007), arXiv:0707.0249 [nucl-th].
 51. J. L. Albacete and A. Dumitru (2010), arXiv:1011.5161 [hep-ph].
 52. C. Salgado, J. Alvarez-Muniz, F. Arleo, N. Armesto, M. Botje *et al.*, *J.Phys.G* **G39**, 015010 (2012), arXiv:1105.3919 [hep-ph].
 53. Y. V. Kovchegov and K. Tuchin, *Phys. Rev.* **D65**, 074026 (2002), hep-ph/0111362.
 54. A. Dumitru, A. Hayashigaki and J. Jalilian-Marian, *Nucl. Phys.* **A765**, 464 (2006), arXiv:hep-ph/0506308.
 55. D. Kharzeev, E. Levin and M. Nardi, *Phys. Rev.* **C71**, 054903 (2005), hep-ph/0111315.
 56. D. Kharzeev, E. Levin and M. Nardi, *Nucl. Phys.* **A747**, 609 (2005), arXiv:hep-ph/0408050.
 57. D. Kharzeev, E. Levin and M. Nardi (2007), arXiv:0707.0811 [hep-ph].
 58. J.-P. Blaizot, T. Lappi and Y. Mehtar-Tani, *Nucl.Phys.* **A846**, 63 (2010), arXiv:1005.0955 [hep-ph].
 59. R. Baier, A. Mueller, D. Schiff and D. Son (2011), arXiv:1103.1259 [nucl-th], * Temporary entry *.
 60. B. Schenke, P. Tribedy and R. Venugopalan, *Phys.Rev.* **C86**, 034908 (2012), arXiv:1206.6805 [hep-ph].
 61. A. Dumitru and L. D. McLerran, *Nucl. Phys.* **A700**, 492 (2002), hep-ph/0105268.
 62. E. Levin and A. H. Rezaeian, *Phys. Rev.* **D83**, 114001 (2011), arXiv:1102.2385 [hep-ph].
 63. A. Dumitru, D. E. Kharzeev, E. M. Levin and Y. Nara, *Phys.Rev.* **C85**, 044920 (2012), arXiv:1111.3031 [hep-ph].
 64. P. Tribedy and R. Venugopalan, *Phys.Lett.* **B710**, 125 (2012), arXiv:1112.2445 [hep-ph].
 65. ALICE Collaboration Collaboration (B. Abelev *et al.*) (2012), arXiv:1210.3615 [nucl-ex].
 66. A. H. Rezaeian, *Phys.Rev.* **D85**, 014028 (2012), arXiv:1111.2312 [hep-ph].
 67. BRAHMS Collaboration (I. Arsene *et al.*), *Phys. Rev. Lett.* **93**, 242303 (2004), arXiv:nucl-ex/0403005.
 68. STAR Collaboration (J. Adams *et al.*), *Phys. Rev. Lett.* **97**, 152302 (2006), arXiv:nucl-ex/0602011.
 69. D. Kharzeev, Y. V. Kovchegov and K. Tuchin, *Phys.Rev.* **D68**, 094013 (2003), arXiv:hep-ph/0307037 [hep-ph].
 70. J. L. Albacete, N. Armesto, A. Kovner, C. A. Salgado and U. A. Wiedemann, *Phys.Rev.Lett.* **92**, 082001 (2004), arXiv:hep-ph/0307179 [hep-ph].
 71. C. Marquet, *Nucl. Phys.* **A796**, 41 (2007), arXiv:0708.0231 [hep-ph].
 72. B. Z. Kopeliovich, J. Nemchik, I. K. Potashnikova, M. B. Johnson and I. Schmidt, *Phys. Rev.* **C72**, 054606 (2005), arXiv:hep-ph/0501260.
 73. L. Frankfurt and M. Strikman, *Phys. Lett.* **B645**, 412 (2007).
 74. ALICE Collaboration Collaboration (B. Abelev *et al.*) (2012), arXiv:1210.4520 [nucl-ex].
 75. A. H. Rezaeian, *Phys.Lett.* **B718**, 1058 (2013), arXiv:1210.2385 [hep-ph].
 76. Z.-B. Kang, I. Vitev and H. Xing, *Phys.Lett.* **B718**, 482 (2012), arXiv:1209.6030 [hep-ph].
 77. R. Xu, W.-T. Deng and X.-N. Wang, *Phys.Rev.* **C86**, 051901 (2012),

- arXiv:1204.1998 [nucl-th].
78. J. L. Albacete and C. Marquet, *Phys. Lett.* **B687**, 174 (2010), arXiv:1001.1378 [hep-ph].
 79. J. Jalilian-Marian and Y. V. Kovchegov, *Phys. Rev.* **D70**, 114017 (2004), hep-ph/0405266.
 80. N. N. Nikolaev, W. Schafer, B. G. Zakharov and V. R. Zoller, *Phys. Rev.* **D72**, 034033 (2005), arXiv:hep-ph/0504057.
 81. R. Baier, A. Kovner, M. Nardi and U. A. Wiedemann, *Phys. Rev.* **D72**, 094013 (2005), arXiv:hep-ph/0506126.
 82. K. Tuchin, *Nucl.Phys.* **A846**, 83 (2010), arXiv:0912.5479 [hep-ph].
 83. J. L. Albacete and C. Marquet, *Phys.Rev.Lett.* **105**, 162301 (2010), arXiv:1005.4065 [hep-ph].
 84. A. Stasto, B.-W. Xiao and F. Yuan (2011), arXiv:1109.1817 [hep-ph].
 85. E. Braidot and f. t. S. collaboration (2010), arXiv:1005.2378 [hep-ph].
 86. Z.-B. Kang, I. Vitev and H. Xing, *Phys.Rev.* **D85**, 054024 (2012), arXiv:1112.6021 [hep-ph].
 87. J. L. Albacete (2012), arXiv:1209.0336 [hep-ph].
 88. A. Kovner and M. Lublinsky, *JHEP* **0611**, 083 (2006), arXiv:hep-ph/0609227 [hep-ph].
 89. F. Gelis, T. Lappi and L. McLerran, *Nucl.Phys.* **A828**, 149 (2009), arXiv:0905.3234 [hep-ph].
 90. T. Lappi, S. Srednyak and R. Venugopalan, *JHEP* **1001**, 066 (2010), arXiv:0911.2068 [hep-ph].
 91. A. Dumitru and Y. Nara, *Phys.Rev.* **C85**, 034907 (2012), arXiv:1201.6382 [nucl-th].
 92. A. Dumitru and E. Petreska (2012), arXiv:1209.4105 [hep-ph].
 93. Z. Koba, H. B. Nielsen and P. Olesen, *Nucl.Phys.* **B40**, 317 (1972).
 94. UA5 Collaboration Collaboration (R. Ansorge *et al.*), *Z.Phys.* **C43**, 357 (1989).
 95. ALICE Collaboration Collaboration (K. Aamodt *et al.*), *Eur.Phys.J.* **C68**, 89 (2010), arXiv:1004.3034 [hep-ex].
 96. CMS Collaboration Collaboration (V. Khachatryan *et al.*), *JHEP* **1101**, 079 (2011), arXiv:1011.5531 [hep-ex].
 97. J. F. Grosse-Oetringhaus and K. Reygers, *J.Phys.* **G37**, 083001 (2010), arXiv:0912.0023 [hep-ex].
 98. W. A. Zajc, *Phys.Lett.* **B175**, 219 (1986).
 99. A. Dumitru, J. Jalilian-Marian and E. Petreska, *Phys.Rev.* **D84**, 014018 (2011), arXiv:1105.4155 [hep-ph].
 100. T. Hirano, U. W. Heinz, D. Kharzeev, R. Lacey and Y. Nara, *Phys.Lett.* **B636**, 299 (2006), arXiv:nucl-th/0511046 [nucl-th].
 101. H.-J. Drescher, A. Dumitru, A. Hayashigaki and Y. Nara, *Phys.Rev.* **C74**, 044905 (2006), arXiv:nucl-th/0605012 [nucl-th].
 102. H.-J. Drescher, A. Dumitru, C. Gombeaud and J.-Y. Ollitrault, *Phys.Rev.* **C76**, 024905 (2007), arXiv:0704.3553 [nucl-th].
 103. PHOBOS Collaboration Collaboration (B. Alver *et al.*), *Phys.Rev.Lett.* **98**, 242302 (2007), arXiv:nucl-ex/0610037 [nucl-ex].
 104. B. Alver and G. Roland, *Phys.Rev.* **C81**, 054905 (2010), arXiv:1003.0194 [nucl-th].
 105. G.-Y. Qin, H. Petersen, S. A. Bass and B. Muller, *Phys.Rev.* **C82**, 064903 (2010), arXiv:1009.1847 [nucl-th].
 106. ATLAS Collaboration (J. Jia) (2012), arXiv:1209.4232 [nucl-ex].

107. C. Gale, S. Jeon, B. Schenke, P. Tribedy and R. Venugopalan (2012), [arXiv:1209.6330](#) [nucl-th].
108. R. Baier, A. H. Mueller, D. Schiff and D. T. Son, *Phys. Lett.* **B502**, 51 (2001), [hep-ph/0009237](#).
109. D. Kharzeev and M. Nardi, *Phys. Lett.* **B507**, 121 (2001), [nucl-th/0012025](#).
110. The ALICE Collaboration (B. Abelev *et al.*), *Phys. Rev. Lett.* **105**, 252301 (2010), [arXiv:1011.3916](#) [nucl-ex].
111. ALICE Collaboration Collaboration (K. Aamodt *et al.*), *Phys.Rev.Lett.* **106**, 032301 (2011), [arXiv:1012.1657](#) [nucl-ex].
112. Alberica Toia for the ALICE Collaboration Collaboration (A. Toia), *J.Phys.G* **G38**, 124007 (2011), [arXiv:1107.1973](#) [nucl-ex].
113. CMS Collaboration Collaboration (S. Chatrchyan *et al.*) (2012), [arXiv:1205.2488](#) [nucl-ex].
114. M. Gyulassy, Y. Pang and B. Zhang, *Nucl.Phys.* **A626**, 999 (1997), [arXiv:nucl-th/9709025](#) [nucl-th].
115. K. Eskola, K. Kajantie, P. Ruuskanen and K. Tuominen, *Nucl.Phys.* **B570**, 379 (2000), [arXiv:hep-ph/9909456](#) [hep-ph].
116. A. Dumitru and M. Gyulassy, *Phys.Lett.* **B494**, 215 (2000), [arXiv:hep-ph/0006257](#) [hep-ph].
117. A. Kovner and M. Lublinsky (2012), [arXiv:1211.1928](#) [hep-ph].
118. A. Dumitru, F. Gelis, L. McLerran and R. Venugopalan, *Nucl.Phys.* **A810**, 91 (2008), [arXiv:0804.3858](#) [hep-ph].
119. STAR Collaboration Collaboration (J. Adams *et al.*), *Phys.Rev.Lett.* **95**, 152301 (2005), [arXiv:nucl-ex/0501016](#) [nucl-ex].
120. STAR Collaboration Collaboration (B. Abelev *et al.*), *Phys.Rev.* **C80**, 064912 (2009), [arXiv:0909.0191](#) [nucl-ex].
121. PHOBOS Collaboration Collaboration (B. Alver *et al.*), *Phys.Rev.Lett.* **104**, 062301 (2010), [arXiv:0903.2811](#) [nucl-ex].
122. CMS Collaboration Collaboration (S. Chatrchyan *et al.*), *Physics Letters B* (2012), [arXiv:1210.5482](#) [nucl-ex].
123. ALICE Collaboration Collaboration (B. Abelev *et al.*) (2012), [arXiv:1212.2001](#) [nucl-ex].
124. ATLAS Collaboration Collaboration (G. Aad *et al.*) (2012), [arXiv:1212.5198](#) [hep-ex].
125. K. Dusling and R. Venugopalan (2012), [arXiv:1211.3701](#) [hep-ph].
126. A. Kovner and M. Lublinsky, *Phys.Rev.* **D83**, 034017 (2011), [arXiv:1012.3398](#) [hep-ph].
127. A. Kovner and M. Lublinsky, *Phys.Rev.* **D84**, 094011 (2011), [arXiv:1109.0347](#) [hep-ph].
128. Y. V. Kovchegov and D. E. Wertepny (2012), [arXiv:1212.1195](#) [hep-ph].
129. A. Dumitru, *RBRC workshop 'Progress in High-pT Physics at RHIC'*, <http://www.bnl.gov/riken/php/agenda.htm> (march 17-19, 2010).
130. K. Dusling, F. Gelis, T. Lappi and R. Venugopalan (2009), [arXiv:0911.2720](#) [hep-ph].
131. A. Dumitru, K. Dusling, F. Gelis, J. Jalilian-Marian, T. Lappi *et al.*, *Phys.Lett.* **B697**, 21 (2011), [arXiv:1009.5295](#) [hep-ph].
132. K. Dusling and R. Venugopalan, *Phys.Rev.Lett.* **108**, 262001 (2012), [arXiv:1201.2658](#) [hep-ph].